Electrostatic fluctuations in the solar wind: An evidence of the link between Alfvénic and electrostatic scales

A. Vecchio, F. Valentini, S. Donato, V. Carbone, C. Briand, J. Bougeret, P. Veltri

AGU PUBLICATIONS

JGR

Journal of Geophysical Research: Space Physics

RESEARCH ARTICLE

10.1002/2014JA020091

Key Points:
- The paper analyzes solar wind data from STEREO spacecraft
- A significant comparison with kinetic numerical simulations is discussed
- Contribution to the understanding of the energy transfer toward small scales

Correspondence to:
A. Vecchio,
antonio.vecchio@ingv.it

Citation:
Vecchio, A., F. Valentini, S. Donato, V. Carbone, C. Briand, J. Bougeret, and P. Veltri (2014), Electrostatic fluctuations in the solar wind: An evidence of the link between Alfvénic and electrostatic scales, *J. Geophys. Res. Space Physics*, *119*, 7012–7024, doi:10.1002/2014JA020091.

Received 16 APR 2014
Accepted 9 AUG 2014
Accepted article online 14 AUG 2014
Published online 2 SEP 2014

Electrostatic fluctuations in the solar wind: An evidence of the link between Alfvénic and electrostatic scales

A. Vecchio[1,2], F. Valentini[2], S. Donato[2], V. Carbone[2], C. Briand[3], J. Bougeret[3], and P. Veltri[2]

[1]Istituto Nazionale di Geofisica e Vulcanologia - Sede di Cosenza, Rende, Cosenza, Italy, [2]Dipartimento di Fisica, Universitá della Calabria, Rende, Cosenza, Italy, [3]LESIA-Observatoire de Paris, CNRS, UPMC Université Paris 06, Université Paris-Diderot, Meudon, Paris, France

Abstract Electrostatic activity in the frequency range of few kHz represents a very common phenomenon observed in the solar wind since first observation from Helios spacecraft. In this paper we present a detailed comparison between electrostatic fluctuations detected by STEREO spacecraft and the results of kinetic numerical simulations. By using a novel approach, made by a combination of two different numerical models, we provide a convincing interpretation of the space observations in terms of the electrostatic branch of the so-called ion-bulk waves able to survive against Landau damping even at small values of T_e/T_p. The comparison between data and numerical simulations allows to characterize the chain of physical mechanisms, able to efficiently transfer energy from the Alfvénic scales down to scales of the order of the Debye length, through the excitation of the observed electrostatic fluctuations.

1. Introduction

The solar wind, a fully ionized almost collisionless gas generated by the Sun and filling the Heliosphere, represents a natural laboratory to study a variety of intriguing physical phenomena, such as plasma turbulence, magnetic reconnection, particle acceleration [*Bruno and Carbone*, 2005]. One of the open aspects concerning the solar wind dynamics is the evidence that the interplanetary medium is hotter than expected as an expanding gas. Since the cooling of the solar wind is less efficient than expected, one of the main challenging problems is the understanding of the nature of the dissipation mechanisms in such an almost collision-free system. In this framework, the turbulent character of the solar wind plays an important role since it allows a progressive energy transfer from large to small scales. Within this scenario, the energy injected by the Sun at large scale (Alfvénic fluctuations) is channeled toward small scales through a turbulent cascade. Due to nonlinear interactions, small-scale fluctuations are generated thus producing significant modifications of the particle distribution function. A detailed investigation of these phenomena, involving a huge variety of scales separated by more than 8–9 orders of magnitude, needs the joint effort of advanced data from the new generation of spacecraft and direct kinetic simulations of turbulence.

Since the first in situ measurements from the Helios spacecraft, a significant level of electrostatic activity in the frequency range of few kHz has been observed as a common feature in the solar wind. In particular, electrostatic fluctuations in the range from about 1 to 10 kHz have been detected for a large fraction of the time (30–50%) when measurements are extended on time windows of several hours [*Gurnett and Anderson*, 1977; *Gurnett and Frank*, 1978; *Gurnett et al.*, 1979; *Briand*, 2009]. This electrostatic signature cannot be simply interpreted as ion-acoustic waves (IAW) [*Mangeney et al.*, 1999; *Araneda et al.*, 2008; *Matteini et al.*, 2010a, 2010b] since IAW are heavily Landau damped at the low T_e/T_p values typical of the solar wind [*Krall and Trivelpiece*, 1986].

In this paper the physical mechanism leading to the excitation of these electrostatic fluctuations is investigated by comparing electric signals measured by STEREO spacecraft with the results of high-resolution Vlasov numerical simulations. We show that the observed features are a signature of the so-called ion-bulk (IBK) waves [*Valentini et al.*, 2011a], excited through an instability process of the beam-plasma type which efficiently transfers energy from Alfvénic scales (greater than the ion inertial length d_p) to length scales close to the Debye length (where charge separation effects come into play). These waves have phase speed close to v_{thp}, acoustic type dispersion and, at variance with the ion-acoustic waves, they can survive against Landau damping even for small T_e/T_p [*Valentini et al.*, 2011a].

Due to the huge separation (more than 8–9 orders of magnitude) between the involved scales, the numerical description of the energy transfer represents a gigantic challenge. To this purpose we followed a novel approach by combining two different numerical models, Hybrid Vlasov-Maxwell (HVM) [*Valentini et al.*, 2007, 2005] and Vlasov-Yukawa (VY) [*Valentini et al.*, 2011b], describing the dynamics of the solar wind plasma at long ($\simeq 40d_p$) and short ($\simeq$ Debye length) scales, respectively, and covering about five and six decades of scales. When supported by high-resolution data from space, this kind of approach could allow to shade new light on energy transfer and heating in solar wind.

2. The Data Analysis

For the present study we use data from the STEREO mission, consisting of two nearly identical spacecraft STEREO A and STEREO B located at a distance of ~1 AU from the Sun, designed for solar observations and interplanetary space measurements. Data measured in the period March 2007 to December 2009 were analyzed. During this period the mutual distance between STEREO A and B increases from ~0.052° to ~132°. We considered data acquired by three instruments, namely WAVES, In-situ Measurements of Particles and CME Transients (IMPACT), and PLAsma and SupraThermal Ion Composition (PLASTIC) providing in situ measurements of low-frequency electric field, local vector magnetic field, and plasma characteristics of protons, respectively.

WAVES is a radio receptor based on three 6 m long mutually orthogonal monopole antennas with an effective length of about 1 m [*Bougeret et al.*, 2008; *Bale et al.*, 2008]. We used data acquired by the Time Domain Sampler, a broadband waveform sampler that provides measurements of voltage along the antennas [*Bale et al.*, 2008] and captures and stores snapshots of electric waveforms. For our study we use data at two different sampling rates of $\Delta t = 4$ μs and $\Delta t = 8$ μs. Since the number of samples is fixed at 16,384, each event has a total duration of ~ 130 or ~ 65 ms, depending on Δt. This means that the total range of frequencies spanned is in between 0.01 and 125 kHz, namely from below the electron cyclotron frequency (typically 100 Hz in the solar wind) to above the electron plasma frequency (about 10 kHz). We focus on signals characterized by a peak in the electric power in the range $\Delta f = 1$–5 kHz, and according to this requirement 993 events have been selected. We estimated that for the considered electric events the electron plasma frequency falls well outside the frequency range Δf; thus, Langmuir waves are ruled out from our analysis. A filtered voltage $V_{\Delta f}$, accounting for the contribution of the frequencies around the peak, is obtained by applying a pass band filter whose bandwidth corresponds to the full width at half maximum of a Gaussian function fitting the power spectra in the range Δf.

A selection is needed to identify the events affected by density fluctuations. When a wave, associated with density fluctuations and having period longer than the charging time of the spacecraft but shorter than the antennas one, encounters the spacecraft the variations in the measured potential follow the change in plasma density. As a consequence, the measured electric field represents the spacecraft response to density fluctuations (spacecraft polarization) associated with the wave and it is not the true electric field of the wave. The spacecraft polarization, reflecting the different state of charge between the antennas and the body of the spacecraft [*Kellogg et al.*, 2009], induces identical signals on the three antennas and is more effective in the range 0.1 to few kHz [*Henri et al.*, 2011]. Since we want to compare the true electric field of the wave with the results of numerical simulations, events for which $V_{\Delta f}$ shows identical waveforms on the three antennas, thus dominated by the spacecraft polarization in the range Δf, have been excluded from the following analysis. To identify events with identical waveforms, we compared the amplitudes on the three antennas through the ratio R_S between the maximum and minimum value of the standard deviation of $V_{\Delta f}$. Events with R_S sufficiently larger than unity, for which the three antennas do not show identical signals, can provide physical information about the electric field in the solar wind since the contribution of density fluctuations is not dominant. The distribution of R_S for the 993 events is shown in Figure 1 (black line). For comparison, we also show the same distribution for the voltage V_{low} (red line), filtered between 0.3 and 0.8 kHz in which the density fluctuations are dominant [*Henri et al.*, 2011]. About the 55% of $V_{\Delta f}$ waveforms shows R_S higher than 2.5 while the percentage is reduced to 5% for V_{low}. To exclude signals strongly influenced by density fluctuations in the bandwidth Δf, we choose events characterized by $R_S > 4$. This selection reduces the number of available waveforms to 196. The selection procedure, based only on the similarity of the waveforms on the three antennas, ensures that signals strongly affected by spacecraft polarization are excluded since only events with significantly different amplitudes

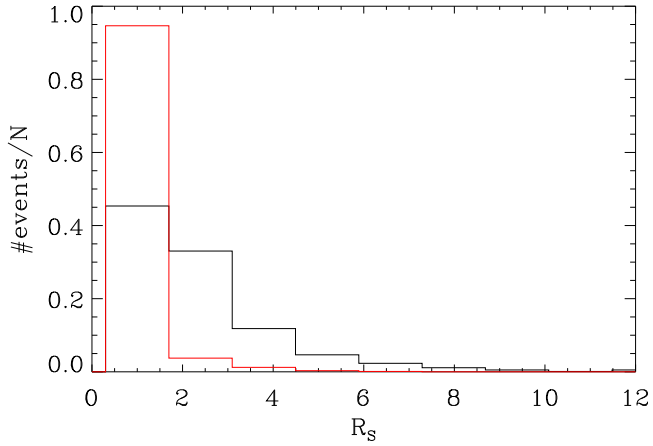

Figure 1. Histogram of R_S, quantifying the contribution of the density fluctuation to the electric signal, for the 993 selected events calculated for $V_{\Delta f}$ (black line) and V_{low} (red line).

on the three antennas are considered. This procedure allows to identify and save only waveforms whose electric field is the true electric field of the solar wind and is not affected by spacecraft disturbances.

For these events the voltage $V_{\Delta f}$ is converted into the corresponding electric field in the spacecraft coordinate system through the set of parameters called w/base caps (Graz), to take into account the effective length and orientation of the STEREO antennas [*Bale et al.*, 2008]. The polarization properties of the electric fluctuations are investigated by rotating the electric field into the minimum variance reference frame [*Sonnerup and Scheible*, 1998; *Graham et al.*, 2014]. The latter has one of the axes aligned with the direction along which the electric field has the largest fluctuations. Being E_i the electric field components along the axes of the spacecraft reference frame, eigenvectors $\mathbf{e}_j$ of the variance matrix $S_{ij} = \langle E_i E_j \rangle - \langle E_i \rangle \langle E_j \rangle$ represent the axes of the new reference system and eigenvalues λ_i indicate the variance along these axes.

Figure 2 shows the distribution of the normalized eigenvalues $\lambda_i/(\lambda_1 + \lambda_2 + \lambda_3)$ and clearly indicates that λ_1 is dominant and well separated from λ_2 and λ_3. The minimum variance analysis on the 196 electric fields indicates that for each event the electric fluctuations are mainly concentrated along the direction $\mathbf{e}_1$, thus implying a linear polarization for the electric signals.

The simultaneous measurements of voltage and magnetic field performed by STEREO allow to investigate the direction of electric fluctuations with respect to the ambient magnetic field $\mathbf{B}_0$. The sampling rate of the magnetic field data measured by the IMPACT magnetometer is 0.125 s, so that about 1 magnetic field value is available for each electric event. For our analysis we chose the value of the magnetic field closest in time to the selected electric event. The angle θ between magnetic field and electric fluctuations, filtered in the range 1–5 kHz, has been calculated from the scalar product in the antennas reference frame. The distribution of $\cos\theta$ for the 196 events, shown in Figure 3, is peaked around $\cos\theta = 1$, and the 73% of the events is characterized by $\theta < 30°$, thus indicating that the electric field fluctuations are mainly directed along the average magnetic field.

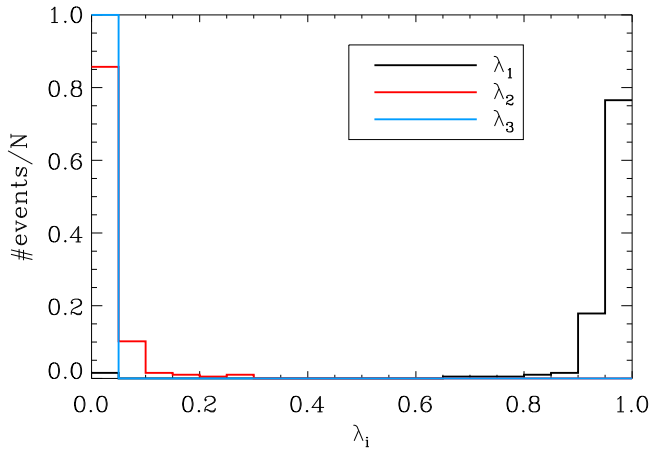

Figure 2. Histogram of the normalized eigenvalues $\lambda_i/(\lambda_1 + \lambda_2 + \lambda_3)$ ($i = 1, 2, 3$) for the 196 selected events (see the text for details).

The solar wind velocity V_{SW}, the temperature T_p, the density n_p, and the thermal speed v_{thp} of protons for the 196 events are available from PLASTIC at 1 min sampling rate. Due to the difference in time resolution, also in this case, we chose the values closest in time to each electric event. In order to set the parameters of the numerical simulations (as explained in the following section) we show the distribution of the proton plasma β_p and the distribution of the ratio between the proton skin depth d_p and the proton Debye length λ_{Dp} (Figures 4 and 5). We recall that $\beta_p = 2v_{\text{thp}}^2/V_A^2$, where $V_A = B_0/\sqrt{4\pi n_p m_p}$ is the Alfvén

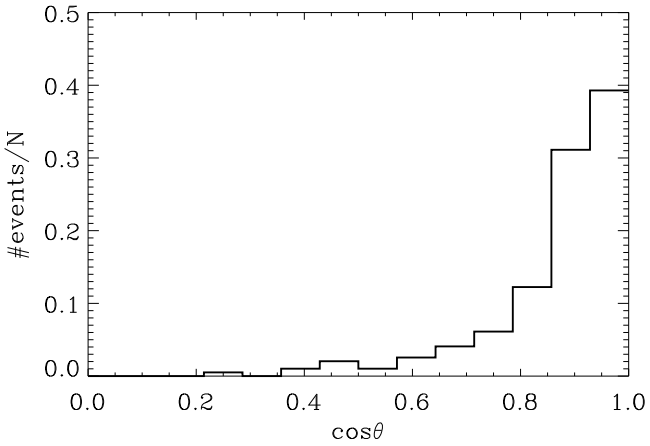

Figure 3. Histogram of cos θ for the 196 selected events (see the text for details).

speed, $\lambda_{Dp} = v_{thp}/\omega_p$, where $\omega_p = \sqrt{4\pi n_p e^2/m_p}$ is the plasma frequency, $d_p = V_A/\Omega_{cp}$, where Ω_{cp} is the proton gyrofrequency. For the considered events β_p has a very well-defined peak at ~1 (Figure 4).

The distribution of d_p/λ_{Dp} peaks at $d_p/\lambda_{Dp} \approx 2.3 \times 10^4$, and 70% of the events are found in the range $1.5 \times 10^4 < d_p/\lambda_{Dp} < 3 \times 10^4$ (Figure 5).

The characteristic values of the measured parameters from STEREO spacecraft will be used to set the proton plasma beta, and the value of d_p/λ_{Dp} in the numerical simulations, and to rescale observed electric waveforms to simulated ones.

3. The Numerical Experiment

3.1. Physical Scenario and Numerical Strategy

The existence of a turbulent cascade at scales larger than ion inertial length represents an ubiquitous phenomenon in solar wind plasma [*Bruno and Carbone*, 2005]. Recent Eulerian Vlasov simulations suggested that the tail at short wavelengths (shorter than the proton inertial length) of the solar wind turbulent cascade in the direction parallel to the ambient magnetic field is dominated by the presence of a significant level of electrostatic activity [*Valentini et al.*, 2008; *Valentini and Veltri*, 2009; *Valentini et al.*, 2010]. The numerical analysis was based on the results of the so-called hybrid Vlasov-Maxwell (HVM) code [*Valentini et al.*, 2007], in which the Vlasov equation is solved for the proton distribution function, while the electrons are treated as a fluid and quasi-neutrality is assumed. In these simulations, the turbulent cascade is triggered by wave-wave interaction processes at large scales (somewhat larger than the proton inertial length d_p) and the role of kinetic effects on protons is analyzed along the cascade up to the range of wavelengths shorter than d_p. These HVM simulations have been carried out both in 1D-3V (one dimension in physical space and three dimensions in velocity space) and in 2D-3V phase space configuration. The physical interpretation of the numerical results showed that along the turbulent cascade the resonant interaction of protons with left-handed polarized Alfvén cyclotron fluctuations generates diffusive plateaus (or small bumps) in the longitudinal velocity distribution [*Kennel and Engelmann*, 1966]. For values of the proton plasma beta of order unity, typical value of the solar wind plasma away from the Sun, this diffusive plateau is generated in the range of velocities close to the proton thermal speed v_{thp} and to the Alfvèn speed (since $\beta_p \sim 1$) [*Valentini et al.*, 2011a]. Beams at longitudinal velocity close to the Alfvèn speed represent a salient feature of the fast solar wind [see, for example, *Marsch*, 2006, and references therein]. Thanks to the presence of bumps, a branch of electrostatic fluctuations (called ion-bulk waves) can be excited through an instability process of the beam-plasma type. IBK waves have phase speed close to v_{thp}, acoustic type dispersion; and at variance with the well-known ion-acoustic waves,

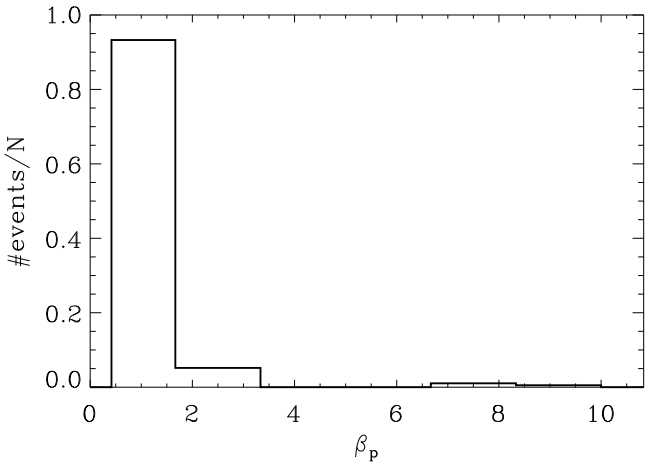

Figure 4. Histogram of plasma β_p for the 196 events.

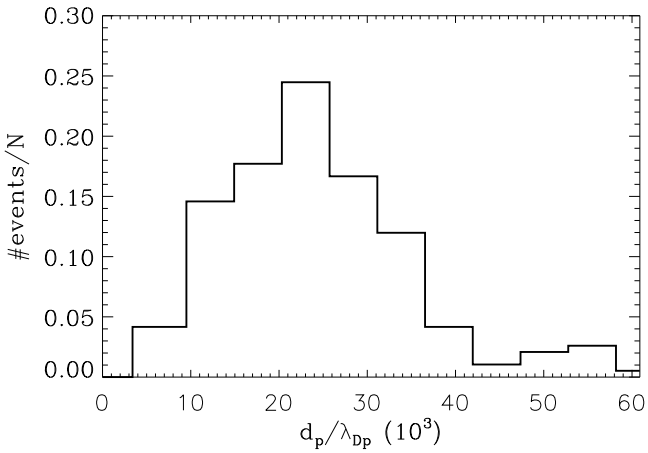

Figure 5. Histogram of d_p/λ_{Dp}, the ratio between the proton skin depth and the Debye length, for the 196 selected events.

they can survive against Landau damping even for low values of the electron to proton temperature ratio [*Valentini et al.*, 2011a]. For these reasons, these fluctuations appear particularly efficient in channeling the energy toward short wavelengths along the solar wind cascade. In the HVM simulations mentioned above, the level of the magnetic fluctuations at wavelengths shorter than d_p results typically 5–7 orders of magnitude lower than that of the electric fluctuations, this means that the system dynamics at such short wavelengths is electrostatic in nature.

The general features of the IBK waves have been deeply investigated in *Valentini et al.* [2011b, 2011c] by means of electrostatic Vlasov-Yukawa (VY) simulations. Within the VY model, the Vlasov equations is solved for the protons, the electron response is taken to be the standard linear Boltzmann response, but charge separation effects, ruled out from the HVM model, are retained. In these simulations, the bump in the proton velocity distribution, needed for the excitation of the ion-bulk fluctuations, is generated by an external electric field applied to the plasma that flattens the velocity distribution at $v \simeq v_{thp}$ through a particle trapping process. The effect of the external electric field in the electrostatic VY simulations is to mimic the resonant interaction of protons with cyclotron fluctuations that produces diffusive plateaus in the longitudinal velocity distribution in the HVM simulations.

From the considerations above, one realizes that the HVM code can reproduce the excitation of the ion-bulk waves by involving typical ingredients of the solar wind medium (cyclotron resonance) but it is limited at short wavelengths by the quasi-neutrality approximation. On the other hand, the VY code can well describe the features of the ion-bulk waves up to length scales where charge separation effects come into play, but it needs an artificial external driver electric field to trigger their excitation. Therefore, the results of HVM simulations and VY simulations are complementary, but the link between the different physical regimes described by HVM and VY models is missed. Nevertheless, on the basis of the results shortly mentioned above, according to which the transfer of energy from large to short wavelengths in the longitudinal direction is driven by a nonlocal instability process, one can think of using a combination of HVM and VY codes to reproduce the evolution of the longitudinal turbulent cascade in the realistic conditions of the interplanetary medium. Therefore, the regime of large wavelengths can be described by the HVM model to reproduce the resonant cyclotron interaction and the generation of the small bump in the longitudinal proton velocity distribution in the vicinity of v_{thp}. Then, since we expect that at wavelengths shorter than d_p the system dynamics is governed by electrostatic activity, the numerical analysis might be continued through the electrostatic VY code up to short scales including charge separation effects.

Of course, due to the gigantic scale separation between fluid and kinetic regimes in the solar wind, an intermediate range of wavelengths cannot be described by the combination of HVM and VY simulations (as discussed above for the STEREO data in Figure 5, the proton skin depth and the proton Debye length are separated typically by a factor of $\sim 2 \times 10^4$). Nevertheless, since the excitation of the ion-bulk fluctuations is the result of a nonlocal instability process, one can assume that the intermediate range of spatial scales does not play any peculiar role.

3.2. Setup of the Numerical Simulations

As discussed in the previous section, the evolution of the solar wind turbulent cascade, in the range of wavelengths around the proton skin depth d_p, can be described numerically by making use of the

HVM code. The HVM code integrates numerically the following hybrid Vlasov-Maxwell equations in dimensionless form:

$$\frac{\partial f}{\partial t} + \mathbf{v}\cdot\nabla f + (\mathbf{E} + \mathbf{v}\times\mathbf{B})\cdot\nabla_v f = 0$$
$$\mathbf{E} = -\mathbf{u}\times\mathbf{B} + \frac{1}{n}\mathbf{j}\times\mathbf{B} - \frac{1}{n}\nabla P_e$$
$$\nabla\times\mathbf{E} = -\frac{\partial\mathbf{B}}{\partial t};\quad \nabla\times\mathbf{B} = \mathbf{j} \tag{1}$$

where $f(\mathbf{x}, \mathbf{v}, t)$ is the proton distribution function, $\mathbf{E}(\mathbf{x}, t)$ the electric field, and $\mathbf{B}(\mathbf{x}, t)$ the magnetic field. The proton density n and the ion-bulk velocity $\mathbf{u}$ are obtained as the velocity moments of f. Quasi-neutrality is assumed ($n = n_p = n_e$), and an isothermal equation of state for the electron pressure P_e is chosen to close the above set of HVM equations. We point out that the choice of isothermal electrons is appropriate to describe the propagation of the ion-bulk waves at phase speed close to v_{thp}. In equation (1) times are scaled by the inverse proton-cyclotron frequency $\Omega_{\mathrm{cp}}^{-1}$, velocities by the Alfvén speed V_A, lengths by the proton skin depth $d_p = c/\omega_p = V_A/\Omega_{\mathrm{cp}}$ (c is the speed of light and ω_p the proton plasma frequency), and masses by the proton mass m_p.

In this work the above equations are solved numerically in 1D-3V phase space configuration. We simulate a collisionless plasma, embedded in a uniform magnetic field $\mathbf{B}_0 = B_0\mathbf{e}_x$ (x being the direction of wave propagation). The initial equilibrium consists of a plasma of protons (and fluid electrons) with homogeneous density and Maxwellian distribution of velocities. The proton plasma beta is chosen to be $\beta_p = 2v_{\mathrm{thp}}^2/V_A^2 = 0.5$ ($v_{\mathrm{thp}} = 0.5$ in scaled units), in agreement with the data from STEREO (see Figure 4), and the electron to proton temperature ratio is set to be $T_e/T_p = 1$. Such a low value of T_e/T_p has been chosen in order to study the most unfavorable situation for detecting sound-like electrostatic fluctuations.

Periodic boundary conditions are implemented in physical space. The total length of the simulation box in physical space for this HVM simulation is $L_{\mathrm{HV}} = 2\pi \times 6.4 d_p \simeq 40 d_p$, discretized by $N_x = 2048$ grid points. To trigger the energy cascade, the initial equilibrium is perturbed by a spectrum of Alfvénic fluctuations, left-hand polarized in the plane perpendicular to the background magnetic field and propagating along it. The first three modes in the spectrum of velocity and magnetic fluctuations are excited at $t = 0$ with wave numbers parallel to $\mathbf{B}_0$ in the range $0.15 \lesssim k d_p \lesssim 0.45$ ($k = m k_0 = m 2\pi/L_{\mathrm{HV}}, m = 1, 2, 3$). The root-mean-square of the initial perturbations is about 0.25. This initial condition tries to reproduce the presence and the dynamical evolution of the so-called slab turbulence [*Matthaeus et al.*, 1986; *Carbone et al.*, 1995], characterized by fluctuations with wave vectors mainly along the direction of the ambient magnetic field and propagating outward from the Sun. The presence of this kind of fluctuations in the tail of the MHD solar wind spectrum is likely in that also starting with an isotropic wave vector distribution in a 2-D HVM simulation [*Valentini et al.*, 2010], a spectrum characterized by wave vectors mainly longitudinal and perpendicular with respect to the average magnetic field is obtained when approaching the ion inertial length. The limits of the velocity domain in each direction are fixed at $v^{\max} = \pm 5 v_{\mathrm{thp}}$. Outside the velocity interval in each direction the proton distribution is set equal to zero. The velocity space is discretized by 81^3 grid points.

No density disturbances are imposed on the initial equilibrium at $t = 0$, but, since the initial Alfvénic perturbations do not satisfy the $B^2 = \mathrm{const}$ condition, in the early stage of the system evolution ponderomotive effects produce large wavelength density fluctuations of amplitude $\delta n_p/n_{0p} \simeq 0.1$ (see *Valentini et al.* [2008] for more details).

The HVM simulation is run up to the time when the resonant interaction of protons with left-hand cyclotron waves generates a small bump in the longitudinal velocity distribution of protons at $v \simeq v_{\mathrm{thp}}$ [*Valentini et al.*, 2008; *Valentini and Veltri*, 2009]. At the top in Figure 6, we report in semilogarithmic plot the early time evolution (up to $t = 100\Omega_{\mathrm{cp}}^{-1}$) of the longitudinal electric energy at small scales evaluated as $\mathcal{E}(t) = \sum_k |E_{k_x}|^2$ with $k > 10 d_p^{-1}$. It is clear from this figure that, during the system evolution, $\mathcal{E}$ displays a sudden exponential growth, triggered by an instability process of the beam-plasma type [*Valentini et al.*, 2011c], and then a saturation phase. The HVM simulation is arrested at $t = 40\Omega_{\mathrm{cp}}^{-1}$, right before the occurrence of the beam-plasma instability that would produce the excitation of the ion-bulk fluctuations (the instant of time at which the HVM simulation is arrested is indicated in Figure 6 by the red vertical line).

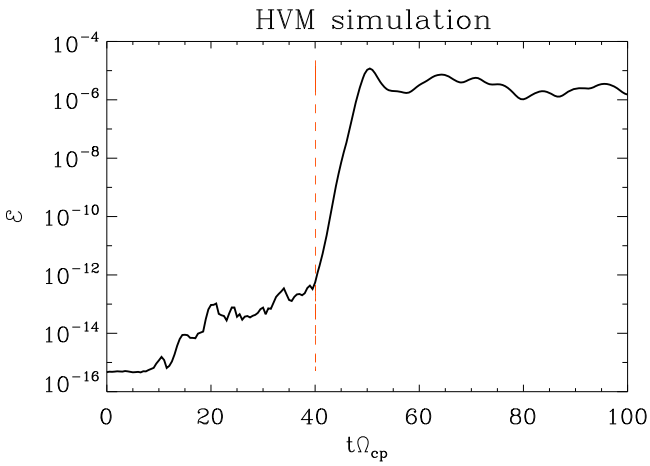

Figure 6. Time evolution of the spectral electric energy at short scales $\mathcal{E}$ from the HVM simulation. The red vertical dashed line represents the time instant at which the HVM simulation is arrested.

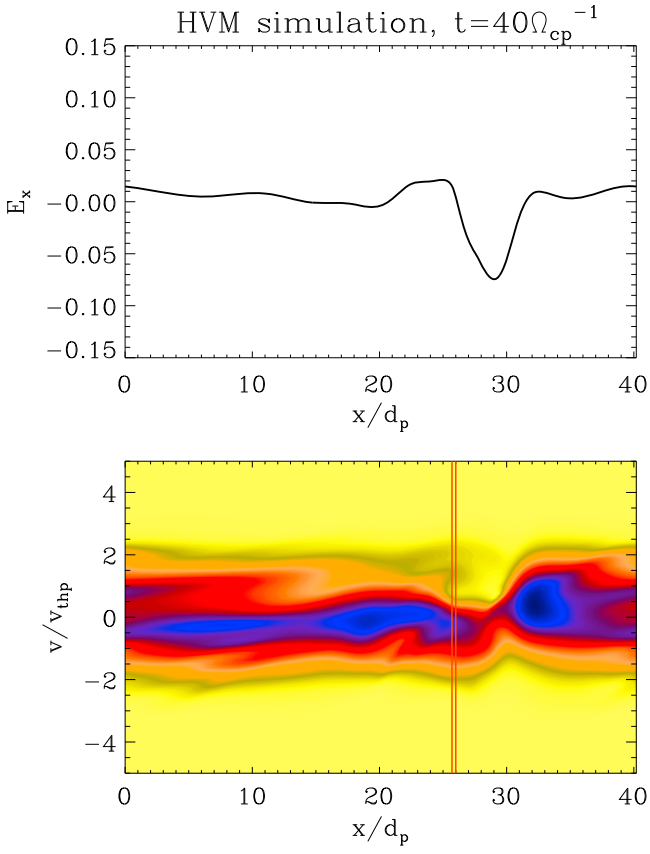

Figure 7. (top) Spatial dependence of the electric field component parallel to the background magnetic field at $t = 40\Omega_{cp}^{-1}$ from the HVM simulation. (bottom) Longitudinal phase space proton distribution function at $t = 40\Omega_{cp}^{-1}$ from the HVM simulation. Vertical red lines indicate the interval over which the proton distribution function is averaged.

Figure 7 (top) shows the electric field signal parallel to $\mathbf{B}_0$ as a function of x/d_p at $t = 40\Omega_{cp}^{-1}$ and the corresponding longitudinal (x, v_x) phase space proton distribution function integrated over v_y and v_z (Figure 7, bottom). Figure 7 represents a significant snapshot of the system before the occurrence of the instability, whose preliminary signatures are already visible in the electric structure generated at $20 \le x/d_p \le 30$ and in the corresponding deformation of the proton distribution at the same spatial location.

At this point, we freeze the HVM simulations at $t = 40\Omega_{cp}^{-1}$ and continue the analysis by means of the electrostatic VY code, starting from the instant of time at which the HVM simulation has been arrested. The use of an electrostatic code to describe the plasma dynamics at wave vectors larger than $\sim 10\, d_p^{-1}$ is also supported by space plasma observations, showing that in this range of scales the effect of the electric field largely prevails over the effects due to the magnetic fields [*Bale et al.*, 2005; *Kellogg et al.*, 2006]. The VY code integrates numerically the Vlasov equation for the proton distribution function coupled to the Yukawa equation for the electrostatic potential, in 1D-1V phase space configuration. The Yukawa equation is derived from the Poisson equation when the electron density has the standard linear Boltzmann form $n_e \simeq n_{0e}(1 + e\phi/k_B T_e)$ (n_e being the particle density, e the electric charge, and ϕ the electrostatic potential).

In dimensionless form, the VY equations are written as follows:

$$\frac{\partial f}{\partial t} + v\frac{\partial f}{\partial x} - \frac{\partial \phi}{\partial x}\frac{\partial f}{\partial v} = 0; \qquad -\frac{\partial^2 \phi}{\partial x^2} + \frac{T_p}{T_e}\phi = \int_{-\infty}^{+\infty} f\,dv - 1 \tag{2}$$

where $f(x, v, t)$ is the proton distribution function and the electric field is given by $E = -\partial\phi/\partial x$. In the above equations, times are scaled by ω_p^{-1}, velocities by v_{thp}, and lengths by the proton Debye length $\lambda_{Dp} = v_{thp}/\omega_p$. With this choice, the electron Debye length in scaled units is $\lambda_{De} = \sqrt{T_e/T_p}$. For $T_e/T_p = 1$ $\lambda_{Dp} = \lambda_{De}$. Finally, the electric field is normalized to the characteristic field $E_0 = m_p v_{thp}\omega_p/e$.

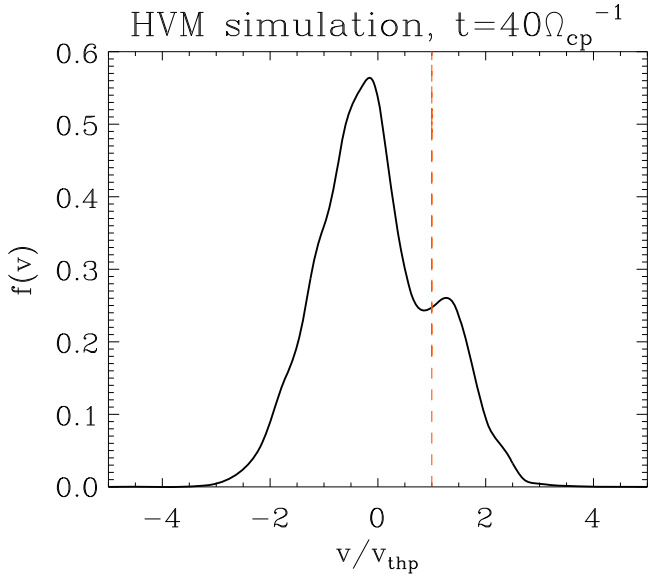

Figure 8. Longitudinal velocity distribution of protons at $t = 40\Omega_{cp}^{-1}$ from the HVM simulation. This velocity profile is obtained by spatial averaging the proton distribution function (integrated over v_y and v_z) over the spatial interval delimited by the two red vertical lines in the bottom plot of Figure 7. Vertical red dashed line represents the value of the proton thermal speed v_{thp}.

As for the HVM simulations, periodic boundary conditions are imposed in physical space and the limits of the numerical velocity interval are fixed at $v^{max} = \pm 5 v_{thp}$. The 1D-1V phase space for the VY simulations is discretized by $N_x = 16,384$ grid points in the spatial domain and $N_v = 1001$ grid points in the velocity domain. The large value of N_x allows us to describe the electric energy spectra on a range of four decades of wave numbers. The total length of the numerical box in physical space is $L_{VY} = 2\pi \times 10^3 \lambda_{Dp}$. We point out that, thanks to the high resolution employed in physical space, the Debye length is well resolved within our simulation box.

By using the typical value of d_p/λ_{Dp} from STEREO shown in Figure 5, one gets $L_{VY}/L_{HV} = (2\pi \times 10^3 \lambda_{Dp})/(2\pi \times 6.4 d_p) \simeq 8 \times 10^{-3} \Rightarrow L_{VY} \simeq 0.3 d_p$. In order to give an idea of the scale separation between HVM and VY simulations, in the contour plot in Figure 7 (bottom), we indicate by two red vertical lines the spatial width of the numerical domain for the VY simulations in units of d_p. In other words, the VY simulation will investigate in great detail the phase space region in between the red vertical lines in Figure 7 (bottom). As it is clear, this phase space region is very thin in the x direction so as to be considered as spatially homogeneous in good approximation. We then calculate, from the HVM simulation, the longitudinal proton velocity profile at $t = 40\Omega_{cp}^{-1}$, as the spatial average (over the interval delimited by the red vertical lines of Figure 7) of the proton distribution function integrated along the transverse velocity directions v_y and v_z. This longitudinal velocity distribution is shown in Figure 8 where one clearly sees the generation of a well-defined bump produced by the proton-cyclotron interaction in the vicinity of the proton thermal speed (vertical line). It is worth to note that in the region around v_{thp}, a positive slope of the velocity distribution occurs.

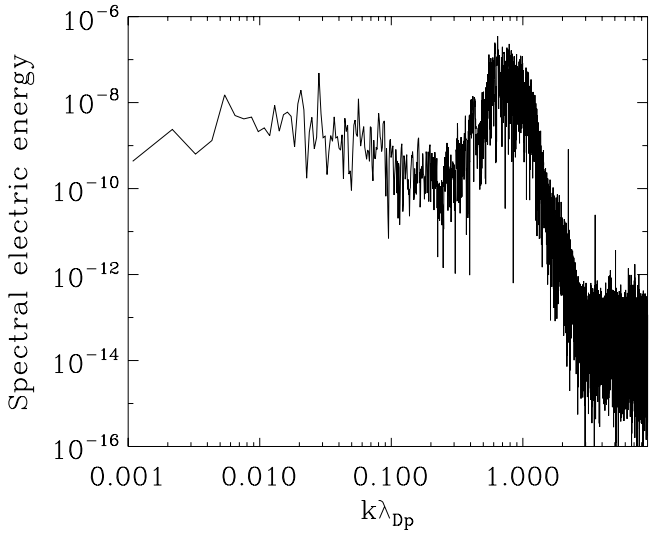

Figure 9. Electric energy spectra of one of the STEREO signals, projected along the maximum variance direction and scaled by E_0, as a function of $k\lambda_{Dp}$. $\lambda_{Dp} \simeq 402$ cm.

The velocity profile in Figure 8 obtained from the HVM simulation at $t = 40\Omega_{cp}^{-1}$ (right before the occurrence of the instability) is then interpolated on a finer velocity grid by a third order spline routine (this ensures the continuity of first and second velocity derivatives of f on the new velocity grid) and used as initial condition for the new electrostatic VY simulation. Initially in the VY simulation, the protons have homogeneous density n_{0p}. We externally impose on the system large wavelength density fluctuations in order to simulate the energy coming from large wavelengths along the cascade. This density noise is imposed on the first three modes of the spectrum in the range of wave numbers

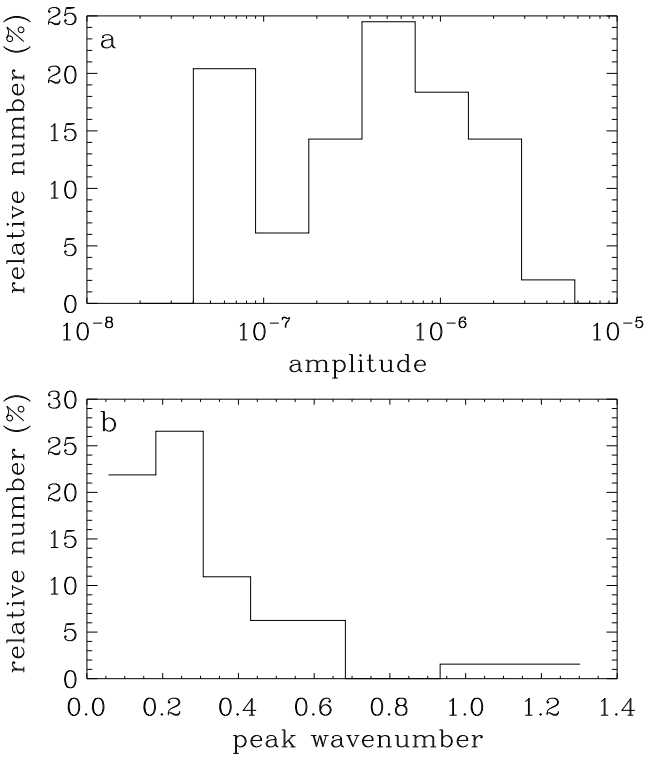

Figure 10. Histogram of the (a) rescaled peak amplitude and (b) peak wave number for the 49 events characterized by $\cos\theta > 0.95$.

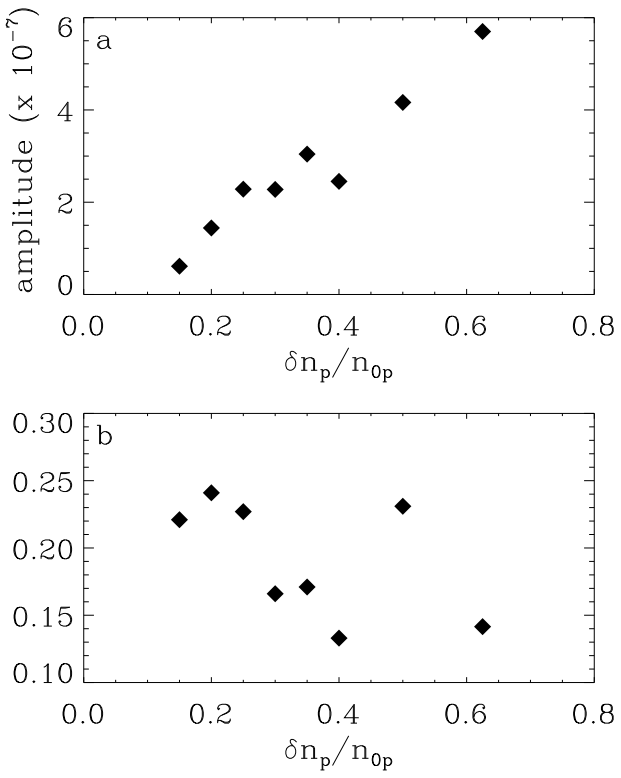

Figure 11. (a) Peak amplitude after the saturation of the instability and (b) peak wave number in the simulated electric spectra as a function of the noise level $\delta n_p/n_{0p}$.

$10^{-3} \lesssim k\lambda_{Dp} \lesssim 3 \times 10^{-3}$, and it is kept on and unchanged during all simulations (mode-freezing large-scale driver), assuming its variation to be slow compared to the time scale of the fluctuations at wavelengths close to λ_{Dp}. As it happens for the HVM simulations (see Figure 6), also in the VY simulations an instability process of the beam-plasma type brings energy from large toward short scales. This instability process displays a saturation phase as it is shown in Figure 6 for the HVM simulation. However, we again point out that, at variance with the HVM simulation, here spatial scales of the order of the Debye length can be reached through the energy cascade.

4. Comparison Between STEREO Data and Numerical Results

The synthetic electric signals obtained through the numerical simulations described above are then compared to the electric waveforms measured by STEREO spacecraft. We remark that the value of $\beta_p = 0.5$ used in the simulations is consistent with observations from STEREO, where we recovered that the 89.7% of the selected events has a proton plasma beta in the range $0.5 \leq \beta_p \leq 1$. In the following we show a comparison between numerical simulations and the 49 STEREO events characterized by $\cos\theta > 0.95$, namely with electric field fluctuations mainly oriented along the average magnetic field, well fitting the physical conditions imposed on the numerical simulations. We remark that the main results of our analysis are unchanged when the full set of 196 events is considered. The measured electric waveforms, time intervals, velocities, and lengths are scaled by the same characteristic parameters used for the VY equations, evaluated from the plasma measurements by PLASTIC. In the solar wind, due to the bulk motion, the measured frequency f_{obs} of the electric signals is Doppler shifted as $f_{obs} = f + (kV_{sw}/2\pi)\cos\theta_{kV}$, where $f = kv_\phi/2\pi$ is the real frequency of the

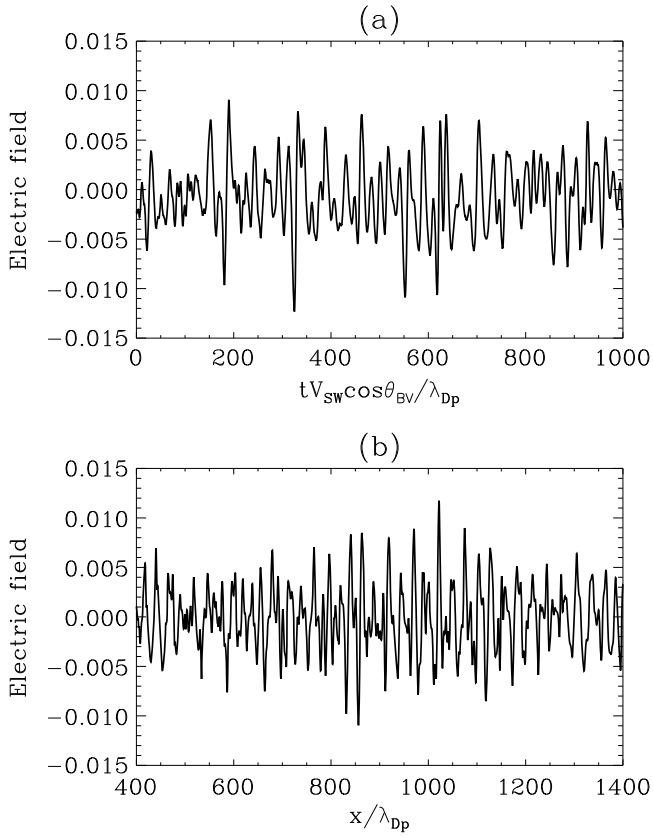

Figure 12. (a) Electric field signal from STEREO projected along the maximum variance direction and scaled by E_0. (b) Electric field signal from the VY simulation after the saturation of the instability.

fluctuations, v_ϕ their phase velocity, and θ_{kV} is the angle between the wave vector and the solar wind speed. Since for the selected events, $\cos\theta \sim 1$ the direction of the wave vectors is close to the direction of the average magnetic field, i.e., $\theta_{kV} \simeq \theta_{BV}$.

By using the Taylor hypothesis, assuming that the wave phase speed of the fluctuations is much smaller than the solar wind velocity, an expression for the wave number $k = 2\pi f_{obs}/(V_{SW}\cos\theta_{BV})$ is found. In this way we can easily pass from time t to space l through the formula $l = tV_{SW}\cos\theta_{BV}$, where θ_{BV} is calculated from the data. In our case the Taylor hypothesis is suitable since the phase velocity of the IBK waves, calculated from the numerical simulations, is close to the proton thermal speed, the latter being about 10 times lower than the V_{SW} as estimated from the PLASTIC data. When represented in the k space, the electric energy spectra display a well-defined peak (Figure 9). In Figures 10a and 10b we show the histograms of the peak amplitude and the corresponding peak wave number for the 49 events, respectively. Peak amplitude and wave number have been evaluated through a Gaussian fitting procedure, which gives rise to an estimated statistical error of 2% (amplitude) and 1% (wave number).

In the VY simulation the amplitude of the electric signals depends on the level of the density noise imposed at large scale, $\delta n_p/n_{0p}$, at $t = 0$. We performed 10 numerical experiments with different amplitudes of the initial density disturbance in the range $0.05 \le \delta n_p/n_{0p} \le 0.625$. Recent high-frequency measurements [*Chen et al.*, 2014] of the solar wind proton density show that the amplitude of the density fluctuation level at frequencies around 10 Hz, corresponding to the wavelengths at which the noise is imposed in the VY simulations, is likely in the solar wind. Moreover, in this range of frequencies the density is strongly intermittent, thus indicating that locally in the solar wind it is possible to find an even higher level of density fluctuations at frequency of ~10 Hz [*Chen et al.*, 2014]. Figure 11 shows peak amplitudes, after the saturation of the instability, and wave number as obtained for different values of density disturbance. Only nine data points are shown because for $\delta n_p/n_{0p} = 0.05$ the instability does not occur. Electric field amplitude (Figure 11a), calculated from the power spectra of selected electric waveforms and rescaled by E_0, increases by increasing the fluctuation level; and the minimum value from data and simulations, $\sim 1.5 \times 10^{-8}$ and $\sim 4 \times 10^{-8}$, respectively, is strictly similar. This comparison suggests that the development of electrostatic fluctuation is a threshold phenomenon and explains the very close minimum value between data and simulations. The peak wave number values from simulations (Figure 11b) are restricted to a very small interval between 0.13 and 0.24. Also, this result is in good agreement with the measurements since the 94% of the peak wave number values from STEREO are found in the same range. These values of the peak wave number, found for both data and simulations, can be understood in the framework of the linear Vlasov theory. By using the velocity profile in Figure 8 in a linear Vlasov solver (that numerically computes the Landau complex integral) a wave dispersion relation of the acoustic type, with phase speed close to v_{thp}, and an unstable region of wave numbers are found. The most unstable wave number is $k^* \simeq 0.3$, for $T_e/T_p = 1$; and when increasing T_e/T_p, the value of k^* increases as well. From this simplified approach one can also argue that STEREO events with

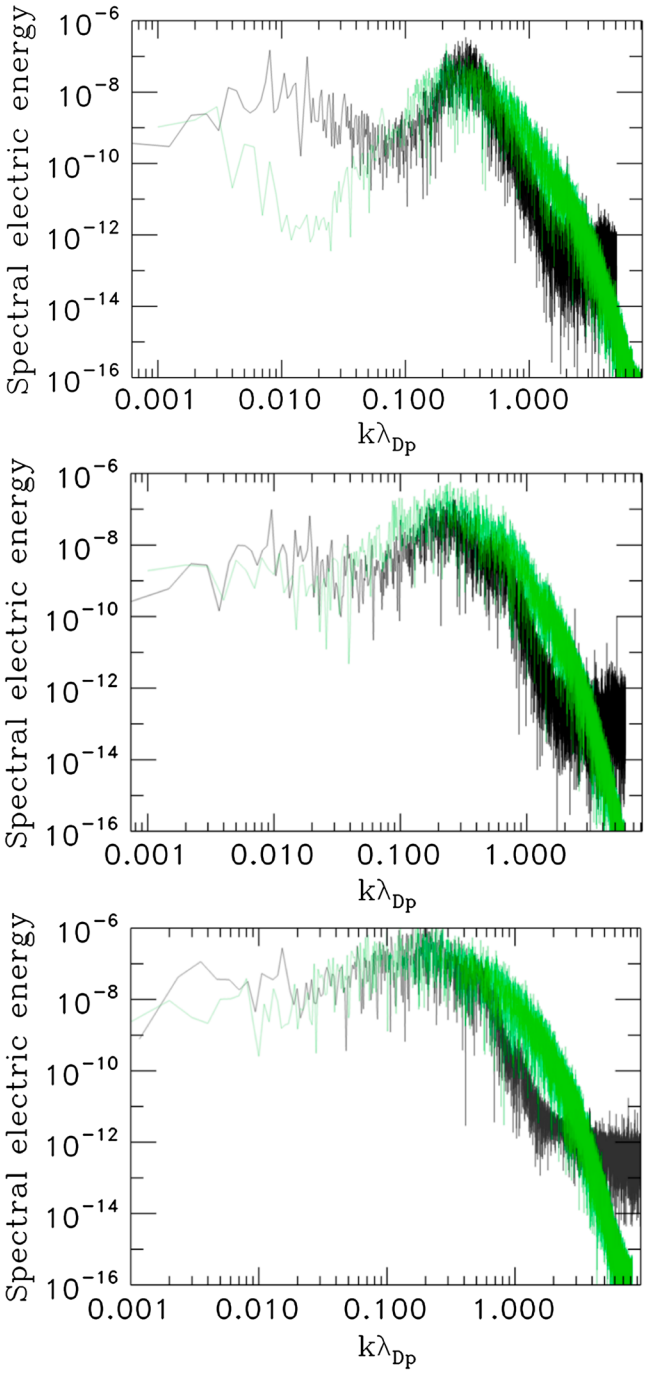

Figure 13. (top to bottom) Electric energy spectra for three STEREO signals projected along the maximum variance direction (black) and the numerical signal (green) as a function of $k\lambda_{Dp}$ for different levels of density disturbances $\delta n_p/n_{0p} = 0.15, 0.25$, and 0.5.

peak wave numbers larger than 0.3 could correspond to situations in which $T_e/T_p > 1$. Unfortunately, since measurements of T_e are not available from STEREO, we cannot be conclusive on this point.

In Figure 12 we show, as an example, the electric field signals of one among the 49 STEREO events, projected along the electric maximum variance direction and scaled by E_0 (Figure 12a), and of a VY simulation with $\delta n_p/n_{0p} = 0.2$, after the saturation of the beam-plasma instability process (Figure 12b), as a function of the normalized spatial coordinate. The two waveforms display the same impulsively spiky behavior and show comparable amplitudes. Moreover, the typical spatial scales of the spikes in the electric waveforms from STEREO are in very good agreement with those obtained from the simulations.

Figure 13 compares the observed (black line) and simulated (green line) electric spectra for different density fluctuation levels (from top to bottom, $\delta n_p/n_{0p} = 0.15, 0.25$, and 0.5). A marked peak is visible in both the energy spectra in the range $0.2 \lesssim k\lambda_{Dp} \lesssim 0.3$. Maximum amplitude of the peak and shapes is significantly comparable for observed and numerical results.

5. Conclusions

Electrostatic fluctuations in the range of frequencies of few kHz, propagating along the background magnetic field, are identified in the high-sampling rate electric fields measured by STEREO. We developed a procedure able to select electric events not affected by the spacecraft polarization, i.e., the spacecraft response to density fluctuations, and thus allowing to investigate the true electric fluctuations of the solar wind. The observed features have been reproduced by high-resolution Vlasov numerical simulations which provide a convincing interpretation of the space observations as a signature of the electrostatic branch of the ion-bulk waves able to survive against Landau damping even at small T_e/T_p. The results of our simulations are safely compared with all the physical parameters which can be derived from STEREO data. Observed electric field waveforms from data and simulations show the same spiky behavior; both amplitudes and typical spatial scales of the spikes are in very good agreement. In the same way, the electric energy spectra from data and simulations, when plotted as a function of the wave number, show significantly comparable shapes and peak values. In order

to perform a quantitative analysis, the peak amplitude and wave number of the measured electric energy spectra have been compared with synthetic spectra generated by varying the density noise level imposed at large scale in the VY simulations. This comparison indicates that the development of electrostatic fluctuations is a threshold phenomenon since the minimum peak amplitude observed in data and simulation is very similar, being $\sim 1.5 \times 10^{-8}$ and $\sim 4 \times 10^{-8}$, respectively. In the same way, the peak wave numbers from data and simulations are in good agreement since the 94% of the values, calculated from the STEREO data, is found in the same range in which the values from the simulations lie.

Our results provide a convincing explanation of the chain of physical mechanisms leading to the excitation of the electrostatic fluctuations since the IBK waves are excited through a beam-plasma type instability able to efficiently transfer energy from the Alfvénic scales ($\gg d_p$) to the Debye length. The followed numerical approach, combining a HVM and VY numerical models to describe the dynamics of the solar wind plasma at long ($\simeq 40 d_p$) and short ($\simeq$ Debye length) scales, respectively, is able to accurately describe the energy transfer from large to short scale covering about five–six decades. The success of our strategy is due to the fact that the energy transfer from large to short wavelengths in the direction parallel to the local magnetic field is realized through a nonlocal instability process of the beam-plasma type. Due to this instability, the energy jumps from large to short wavelengths and the intermediate range of spatial scales does not play any peculiar role. This allowed us to combine two different numerical codes to obtain a self-consistent description of the system dynamics over a large range of scales.

Establishing on space data a strict correlation among phenomena occurring on scales separated by more than five decades is a hard goal to achieve, even taking into account the lack of an efficient way to determine the wave vector distribution at large scale from data. Anyway, our simulations clearly show that a sequence of physical mechanisms, which naturally occur in such kind of media, can give rise to instabilities which generate electric fluctuations whose characteristics fit remarkably well those detected in the solar wind.

Electrostatic fluctuations, observed in the solar wind in the range of frequency from 1 to 10 kHz, could play a relevant role for the solar wind heating, since they produce significant modifications on the proton distribution function. When, in the future, the electron temperatures in correspondence to the electrostatic events and more resolved density data during the same events will be available, further more accurate comparisons could be performed to confirm the physical scenario pictured within our model.

Acknowledgments

The numerical simulations discussed in this paper were performed on the FERMI supercomputer at CINECA (Bologna, Italy), within the European project PRACE Pra04-771. We thank three anonymous Referees for very useful suggestions.

Michael Balikhin thanks Jan Blecki and another reviewer for their assistance in evaluating this paper.

References

Araneda, J. A., E. Marsch, and F. A. Viñas (2008), Proton core heating and beam formation via parametrically unstable Alfvèn-cyclotron waves, *Phys. Rev. Lett.*, *100*, 125003.

Bale, S. D., P. J. Kellogg, F. S. Mozer, T. S. Horbury, and H. Reme (2005), Measurement of the electric fluctuation spectrum of magnetohydrodynamic turbulence, *Phys. Rev. Lett.*, *94*, 215,002.

Bale, S. D., et al. (2008), The electric antennas for the STEREO/WAVES experiment, *Space Sci. Rev.*, *136*, 529–547.

Bougeret, J. L., et al. (2008), S/WAVES: The radio and plasma wave investigation on the STEREO mission, *Space Sci. Rev.*, *136*, 487–528.

Briand, C. (2009), Review on electrostatic structures in the solar wind: Observational considerations, *Nonlinear Processes Geophys.*, *16*, 319–329.

Bruno, R., and V. Carbone (2005), The solar wind as a turbulence laboratory, *Living Rev. Sol. Phys.*, *2*(4), 1–208.

Carbone, V., F. Malara, and P. Veltri (1995), A model for the three-dimensional magnetic field correlation spectra of low-frequency solar wind fluctuations during Alfvènic periods, *J. Geophys. Res.*, *100*, 1763–1778.

Chen, C. H. K., L. Sorriso-Valvo, J. Šafránková, and Z. Němeček (2014), Intermittency of solar wind density fluctuations from ion to electronn scales, *Astrophys. J. Lett.*, *789*, L8.

Graham, D. B., I. H. Cairns, and D. M. Malaspina (2014), Harmonic waves and sheath rectification in type III solar radio bursts, *J. Geophys. Res. Space Physics*, *119*, 723–741, doi:10.1002/2013JA019317.

Gurnett, D. A., and R. R. Anderson (1977), Plasma wave electric fields in the solar wind—Initial results from HELIOS 1, *J. Geophys. Res.*, *82*, 632–650.

Gurnett, D. A., and L. A. Frank (1978), Ion acoustic waves in the solar wind, *J. Geophys. Res.*, *83*, 58–74.

Gurnett, D. A., E. Marsh, W. Pilipp, R. Schwenn, and H. Rosenbauer (1979), Ion acoustic waves and related plasma observations in the solar wind, *J. Geophys. Res.*, *84*, 2029–2038.

Henri, P., N. Meyer-Vernet, C. Briand, and S. Donato (2011), Observations of langmuir ponderomotive effects using the solar terrestrial relations observatory spacecraft as a density probe, *Phys. Plasmas*, *18*, 082308.

Kellogg, P. J., S. D. Bale, F. S. Mozer, T. S. Horbury, and H. Reme (2006), Solar wind electric field in the ion cyclotron frequency range, *Astrophys. J.*, *645*, 704–710.

Kellogg, P. J., K. Goetz, S. J. Monson, S. D. Bale, M. J. Reiner, and M. Maksimovic (2009), Plasma wave measurements with STEREO S/WAVES: Calibration, potential model, and preliminary results, *J. Geophys. Res.*, *114*, A02107, doi:10.1029/2008JA013566.

Kennel, C. F., and F. Engelmann (1966), Velocity space diffusion from weak plasma turbulence in a magnetic field, *Phys. Fluids*, *9*, 2377–2388.

Krall, N. A., and A. W. Trivelpiece (1986), *Principles of Plasma Physics*, San Francisco Press, San Francisco, Calif.

Mangeney, A., C. Salem, C. Lacombe, J. L. Bougeret, C. Perche, R. Manning, P. J. Kellog, K. Goetz, S. J. Monson, and J. M. Bosqued (1999), WIND observations of coherent electrostatic waves in the solar wind, *Ann. Geophys.*, *17*, 307–320.

Marsch, E. (2006), Kinetic physics of the solar corona and solar wind, *Living Rev. Sol. Phys.*, *3*, 1–100.

Matteini, L., S. Landi, M. Velli, and P Hellinger (2010a), Kinetics of parametric instabilities of Alfvèn waves: Evolution of ion distribution functions, *J. Geophys. Res.*, *115*, A09106, doi:10.1029/2009JA014987.

Matteini, L., S. Landi, L. Del Zanna, M. Velli, and P. Hellinger (2010b), Parametric decay of linearly polarized shear Alfvèn waves in oblique propagation: One and two-dimensional hybrid simulations, *Geophys. Res. Lett.*, *37*, L20101, doi:10.1029/2010GL044806.

Matthaeus, W. H., M. L. Goldstein, and J. H. King (1986), An interplanetary magnetic field ensemble at 1 AU, *J. Geophys. Res.*, *91*, 59–69.

Sonnerup, B. U. O., and M. Scheible (1998), Minimum and maximum variance analysis, in *Analysis Methods for Multi-Spacecraft Data*, edited by G. Paschmann and P. Daly, pp. 185–220, Int. Space Sci. Inst., Bern, Switzerland.

Valentini, F., and P. Veltri (2009), Electrostatic short-scale termination of solar-wind turbulence, *Phys. Rev. Lett.*, *202*, 225001.

Valentini, F., P. Veltri, and A Mangeney (2005), A numerical scheme for the integration of the Vlasov–Poisson system of equations in the magnetized case, *J. Comput. Phys.*, *210*, 730–751.

Valentini, F., P. Travnicek, F. Califano, P. Hellinger, and A. Mangeney (2007), A hybrid-Vlasov model based on the current advance method for the simulation of collisionless magnetized plasma, *J. Comput. Phys.*, *225*, 753–770.

Valentini, F., P. Veltri, F. Califano, and A. Mangeney (2008), Cross-scale effects in solar-wind turbulence, *Phys. Rev. Lett.*, *101*, 025006.

Valentini, F., F. Califano, and P. Veltri (2010), Two-dimensional kinetic turbulence in the solar wind, *Phys. Rev. Lett.*, *104*, 205002.

Valentini, F., D. Perrone, and P. Veltri (2011a), Short-wavelength electrostatic fluctuations in the solar wind, *Astrophys. J.*, *39*, 54.

Valentini, F., F. Califano, D. Perrone, F. Pegoraro, and P. Veltri (2011b), New ion-wave path in the energy cascade, *Phys. Rev. Lett.*, *106*, 165002.

Valentini, F., F. Califano, D. Perrone, F. Pegoraro, and P. Veltri (2011c), Excitation of nonlinear electrostatic waves with phase velocity close to the ion-thermal speed, *Plasma Phys. Controlled Fusion*, *53*, 105017.